High-performance chiral mode switching device at 2 μm waveband using photonic crystal waveguide

Kang Li [1, 2], Hejie Peng [1, 2], Siwei Wang [1, 2], Lin Chen [1, 2], and Jian Wang [1, 2, *]

1.Wuhan National Laboratory for Optoelectronics and School of Optical and Electronic Information, Huazhong University of Science and Technology, Wuhan 430074, Hubei, China.

2.Optics Valley Laboratory, Wuhan 430074, Hubei, China

**Corresponding author: jwang@hust.edu.cn.*

Abstract: We experimentally demonstrate a silicon chiral mode switching device by dynamically encircling exceptional point at 2 μm waveband, with high purities (> 95%) for both TE_0 and TE_1 modes in a broad bandwidth (85 nm).

1. Introduction

The non-Hermitian system containing open boundaries has attracted attention in quantum mechanics, thermodynamics, acoustics, and optics, due to their novel physical phenomena, such as exceptional point (EP) [1, 2]. EPs are the degenerate singularities of the eigenvalues in a non-Hermitian system. In photonics, a wide range of optical configurations tailoring gain and loss, including microcavities [3], gratings [4], coupled waveguides [5], and photonic crystals [6], have been presented to provide diversified intriguing effects of EPs such as topological light control [7], sensing enhancement [8], and chiral mode switching [9].

Among them, chiral mode switching has been theoretically and experimentally verified in recent works [9-11]. For these devices, the mode state of the output port only depends on the encircling direction (clockwise and anticlockwise) rather than the input mode. Encircling a moving EP is proposed to shrink the adiabatically changing structure [10]. Then, a new encircling-EP paradigm containing Hamiltonian hopping overcomes path-dependent losses, to enable ultra-high efficiency chiral mode switching [9]. To further shorten the device length, fast parametric evolution along the parameter space boundary of the system Hamiltonian can obtain a more compact structure [11]. Note that these reported chiral mode switching devices are developed in the silicon photonics platform for the telecommunication wavelength. Besides, the 2 μm waveband recently attracts more attention for many important applications. However, enabling high-performance chiral mode switching devices at 2 μm is still a great challenge.

In this paper, we propose a novel silicon structure of high-performance chiral mode switching at 2 μm waveband for the first time by using the double-coupled photonic crystal waveguide. In the non-Hermitian system, the tailored loss is from the reflected loss of the photonic crystal waveguide, which could be adjusted by changing the diameter of the nanohole. Numerical simulation results show that the presented silicon chiral mode switching device has high performance in mode purity (> 98.7%), transmission efficiency (< 0.6 dB), and broad bandwidth (> 500 nm). The chiral mode switching device with favorable performance has been fabricated in the standard silicon photonic platform and provides the basis for high-performance chiral transmission devices (such as optical isolators, optical switches, and optical logic gates).

2. Design and simulation

2.1 Structure design

Fig. 1 illustrates the schematic of the proposed chiral mode switching device, which includes two silicon coupled photonic crystal waveguides. Each photonic crystal waveguide is a silicon-on-insulator (SOI) strip waveguide with a series of nanoholes. Here, we choose the SOI wafer with a 340-nm-thick top-silicon layer, a 2-μm-thick buried-oxide layer, and a 1.5-μm-thick silicon dioxide (SiO_2) upper-cladding. The width of the input waveguide (W_{BIN} = 1.25 μm) is equal to the width of the output waveguide (W_{BOUT} = 1.25 μm). The 1.25-μm-width waveguide supports two modes (TE_0 mode and TE_1 mode) with low loss. The widths of two different photonic crystal waveguides $W_{U(x)}$ and $W_{D(x)}$ are:

$$W_{U(x)} = \begin{cases} w_0 - \Delta w * \sin\left[(x-0)\pi/40\right] & (0 \le x \le 40) \\ w_0 - \Delta w * \cos\left[(x-40)\pi/80\right] & (40 \le x \le 60) \\ w_0 & (60 \le x \le 127) \end{cases} \quad W_{D(x)} = \begin{cases} w_0 & (0 \le x \le 67) \\ w_0 - \Delta w * \sin\left[(x-67)\pi/40\right] & (67 \le x \le 87) \\ w_0 - \Delta w * \cos\left[(x-87)\pi/80\right] & (87 \le x \le 127) \end{cases} \tag{1}$$

where w_0 is 0.6 μm, and Δw is 0.1 μm. x is the propagation distance increases from 0 μm to 127 μm. The pitch of the upper photonic crystal waveguide Λ_U keeps the constant of 0.2 μm, while the pitch of the down photonic crystal waveguide Λ_D and the gap $d_{(x)}$ of two waveguides are varying, which can be given by the following equation:

$$d_{(x)} = \begin{cases} d_0 + d_1 * \left[(x-0)/20\right]^2 & (0 \le x \le 40) \\ d_0 + d_1 * \left\{1+\left[(x-40)/20\right]^2\right\} & (40 \le x \le 60) \\ d_0 + 2 * d_1 & (60 \le x \le 67) \\ d_0 + d_1 * \left\{2-\left[(x-67)/20\right]^2\right\} & (67 \le x \le 87) \\ d_0 + d_1 * \left\{1-\left[(x-87)/40\right]^2\right\} & (87 \le x \le 127) \end{cases} \qquad \Lambda_D = \begin{cases} 0.2\ \mu m & (1 \le n \le 200,\ 291 \le n \le 490) \\ 0.3\ \mu m & (201 \le n \le 208,\ 283 \le n \le 290) \\ 0.4\ \mu m & (209 \le n \le 216,\ 275 \le n \le 282) \\ 0.5\ \mu m & (217 \le n \le 224,\ 267 \le n \le 274) \\ 0.6\ \mu m & (225 \le n \le 232,\ 259 \le n \le 266) \\ 0.7\ \mu m & (233 \le n \le 258) \end{cases} \tag{2}$$

where d_0 is 0.05 μm and d_1 is 0.75 μm. n is the serial number of the corresponding nanoholes. The D_U and D_D are the diameters of photonic crystal nanohole for two waveguides. The duty cycles ($f_U = D_U / \Lambda_U$, $f_D = D_D / \Lambda_D$) is 0.5.

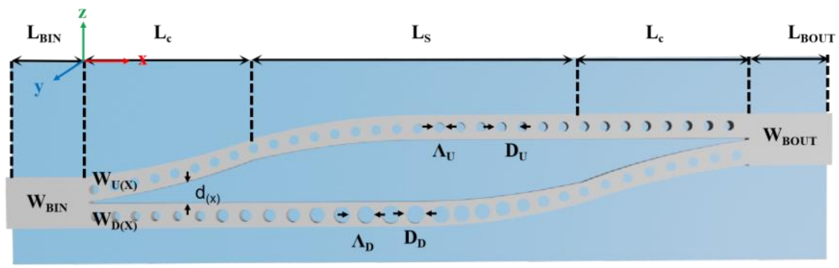

Fig. 1. Schematic of proposed silicon double-coupled photonic crystal waveguides. The device has a 340-nm-thick height and is covered by a 1.5-μm-thick SiO_2 layer. The width of the input waveguide (W_{BIN}) is equal to the width of the output waveguide (W_{BOUT}). $W_{U(X)}$ and $W_{D(X)}$ are the widths of two different photonic crystal waveguides. The Λ_U and Λ_D are the pitches of photonic crystal waveguides. The D_U and D_D are the diameters of photonic crystal nanoholes for two waveguides. The $d_{(x)}$ is the gap of two waveguides.

2.2 Numerical simulation

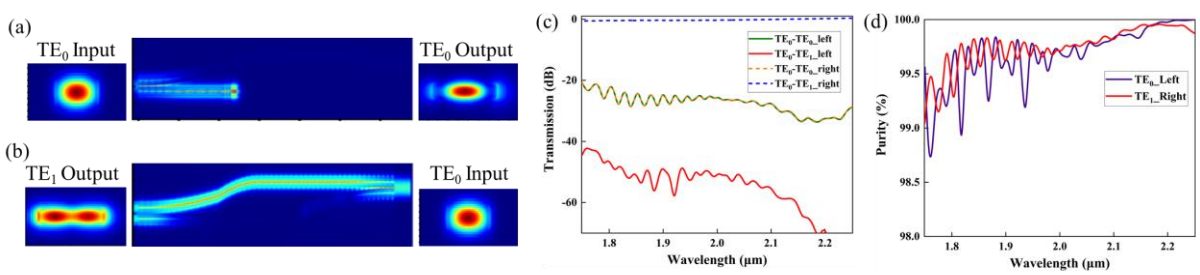

Fig. 2. Simulated normalized electric field distributions at 2 μm waveband, when TE_0 mode inputs from the left port (a) and right port (b), respectively. Calculated results for the TE_0 and TE_1 modes at the output port cover an ultra-broad wavelength range of 1.75-2.25 μm, including (c) transmittance spectra and (d) mode purities.

For the designed chiral mode switching device, a three-dimensional finite-difference time-domain (3D-FDTD) method is used to implement the numerical simulation of light propagation. Fig. 2(a) and (b) show the simulated normalized electric field distributions at 2 μm waveband, when TE_0 mode inputs from the left port and right port, respectively. One can see that when the TE_0 mode is input from the left port, the mode of the output port is TE_0 mode. While the TE_0 mode is incident from the right port, the mode of the output port is TE_1 mode. Fig. 2(c) and (d) display the calculated transmittance spectra and mode purities in an ultra-broad wavelength range of 1.75 - 2.25 μm, respectively. The presented chiral mode switching device could achieve high efficiency of < 0.6 dB and high purities of > 98.7% covering a 500-nm wavelength range.

3. Fabrication and characterization

The designed device is fabricated by utilizing the standard CMOS-compatible fabrication process. The layout pattern is defined using electron-beam lithography (EBL) and inductively coupled plasma (ICP) etching. After that, the grating couplers are shallowly etched down normally 150 nm by another EBL and ICP. Finally, the PECVD (plasma-enhanced chemical vapor deposition) is used to deposit a 1.5-µm-thick SiO_2 upper cladding on the top of the devices. Fig. 3 (a)-(e) show the microscopy images and SEM image of the fabricated high-performance chiral switching device and their test structures, including grating, mode (de)multiplexer, mode (de)multiplexer and chiral mode switching structure, and zoom-in view of chiral mode switching structure.

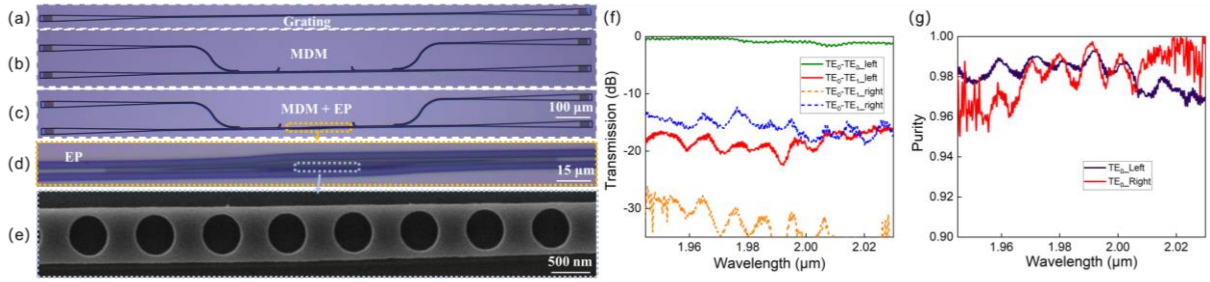

Fig. 3. Microscopy images of the fabricated high-performance chiral switching device and test structures, including (a) grating, (b) mode (de)multiplexer, (c) mode (de)multiplexer and chiral switching structure, and (d) Zoom-in view of chiral switching structure. (e) SEM images of photonic crystal waveguide. Experimental results of the fabricated chiral switching device: (f) transmission spectra, and (g) mode purities.

A 2-µm broadband light source is used as the source and an optical spectrum analyzer (OSA, Yokogawa AQ6375B) is applied as the receiver for the measurement of the transmission spectra at the grating output port. Fig. 3(f) and (g) show the measured transmission spectra and mode purities of the fabricated chiral switching device, respectively. When the TE_0 mode is injected into the left port, the mode of the right output port is TE_0 mode with a high purity of > 95%. While the TE_0 mode is launched from the right port, the mode of the left output port is TE_1 mode with a high purity of > 96% and near-unity transmission efficiency in the wavelength range of 1.945-2.03 µm. The performance of the chiral mode switching device could be improved in the future by further optimizing the fabrication process.

4. Conclusion

In conclusion, a silicon chiral mode switching device at the waveband of 2 µm has been proposed and experimentally demonstrated by utilizing a double-coupled photonic crystal waveguide. The nanohole of the photonic crystal waveguide could be changed to adjust the reflected loss of the waveguide. As a result, the mode states of the output port are different when TE_0 mode is launched from the left or right ports. Simulated results show that such a chiral mode switching device achieves high mode purities of > 98.7% around a bandwidth of 500 nm. The experimental results have shown that the fabricated device has high mode purities of > 95% within the wavelength range of 1945 - 2030 nm. To the best of our knowledge, this is the first high-performance silicon chiral mode switching device working at the waveband of 2 µm. Such device paves the way towards high-purity and ultra-broad chiral transmission devices for a wide range of practical applications at the emerging 2 µm waveband.

5. Funding

This work was supported by the National Natural Science Foundation of China (NSFC) (62125503, 62261160388), the Natural Science Foundation of Hubei Province of China (2023AFA028), and the Innovation Project of Optics Valley Laboratory (OVL2021BG004).

6. References

[1] C. M. Bender et al., “Real Spectra in Non-Hermitian Hamiltonians Having PT Symmetry,” Phys. Rev. Lett. **80**, 5243–5246 (1998).
[2] B. Zhen et al., “Spawning rings of exceptional points out of Dirac cones,” Nature **525**, 354–358 (2015).
[3] L. Feng et al., “Single-mode laser by parity-time symmetry breaking,” Science **346**, 972–975 (2014).
[4] Z. Lin et al., “Unidirectional Invisibility Induced by PT-Symmetric Periodic Structures,” Phys. Rev. Lett. **106**, 213901 (2011).
[5] J. W. Yoon et al., “Time-asymmetric loop around an exceptional point over the full optical communications band,” Nature **562**, 86–90 (2018).
[6] H. Zhou et al., “Exceptional surfaces in PT-symmetric non-Hermitian photonic systems,” Optica **6**, 190-193 (2019).
[7] H. Zhao et al., “Non-Hermitian topological light steering,” Science **365**, 1163-1166 (2019).
[8] W. Chen, “Exceptional points enhance sensing in an optical microcavity,” Nature **548**, 192-196 (2017).
[9] A. Li et al., “Hamiltonian Hopping for Efficient Chiral Mode Switching in Encircling Exceptional Points,” Phys. Rev. Lett. **125**, 187403 (2020).
[10] Q. Liu et al., “Efficient Mode Transfer on a Compact Silicon Chip by Encircling Moving Exceptional Points,” Phys. Rev. Lett. **124**, 153903 (2020).
[11] X. Shu et al., “Fast encirclement of an exceptional point for highly efficient and compact chiral mode converters,” Nat. Commun. **13**, 2123 (2022).